Designing Biomimetic Conductive Gelatin-Chitosan–Carbon Black Nanocomposite Hydrogels for Tissue Engineering

Kamol Dey * , Emanuel Sandrini , Anna Gobetti , Giorgio Ramorino , Luciana Sartore

Posted Date: 23 August 2023

doi: 10.20944/preprints202308.1671.v1

Keywords: hydrogel; gelatin; chitosan; conductive carbon black; nanocomposite; cyclic compression; dissipation energy; anisotropy; tissue engineering

Article

Designing Biomimetic Conductive Gelatin-Chitosan–Carbon Black Nanocomposite Hydrogels for Tissue Engineering

Kamol Dey [1,*], Emanuel Sandrini [2], Anna Gobetti [2], Giorgio Ramorino [2] and Luciana Sartore [2]

[1] Bionanomaterials and Tissue Engineering Laboratory (BNTELab), Department of Applied Chemistry and Chemical Engineering, Faculty of Science, University of Chittagong, Chittagong-4331, Bangladesh
[2] Department of Mechanical and Industrial Engineering, Materials Science and Technology Laboratory, University of Brescia, Via Branze 38, 25123 Brescia, Italy
* Correspondence: kamoldey@cu.ac.bd; kamolacct@gmail.com

Abstract: Conductive nanocomposites play a significant role in tissue engineering by providing a platform to support cell growth, tissue regeneration, and electrical stimulation. In this present study, a set of electroconductive nanocomposite hydrogels based on gelatin (G), chitosan (CH) and conductive carbon black (CB) was synthesized with the aim to develop novel biomaterials for tissue regeneration application. Incorporation of conductive carbon black (10, 15 and 20 wt %) significantly improved electrical conductivity and enhanced mechanical properties with the increased CB content. We employed an oversimplified unidirectional freezing technique to impart anisotropic morphology with interconnected porous architecture. An investigation into whether any anisotropic morphology affects the mechanical properties of hydrogel was conducted by performing compression and cyclic compression tests in each direction parallel and perpendicular to macroporous channels. Interestingly, nanocomposite with 10 % CB produced both anisotropic morphology and mechanical property, whereas anisotropic pore morphology diminished at higher CB concentration (15 and 20 %) imparting denser texture. Collectively, the nanocomposite hydrogels showed great structural stability as well as good mechanical stability and reversibility. Under repeated compressive cyclic at 50 % deformation, the nanocomposite hydrogels showed preconditioning, characteristic hysteresis, nonlinear elasticity, and toughness. Overall, the collective mechanical behavior resembled the mechanics of soft tissues. Electrical impedance associated to the hydrogels was studied in terms of modulus and phase in dry and wet condition. The electrical properties conducted in wet conditions, which is more physiologically relevant, showed low impedance at high frequencies due to capacitive currents. Overall, impedance of the nanocomposite hydrogels decreased with increased CB concentrations. These gelatin-chitosan–carbon black nanocomposite hydrogels show great promise for use as conducting substrates for the growth of electro-responsive cells in tissue engineering.

Keywords: hydrogel; gelatin; chitosan; conductive carbon black; nanocomposite; cyclic compression; dissipation energy; anisotropy; tissue engineering

1. Introduction

Natural extracellular matrix (ECM) is a dynamic, highly complex and hierarchically organized nanocomposites that govern and regulate cells fate and functions [1]. Moreover, the composition, density, nanostructure, and microstructure of ECM vary quite differently between different tissue types [2]. As such, adopting nanotechnological strategy for designing advanced nanocomposites to better emulate the ECM, both architecturally and functionally, has gained intense interests [3]. Tissue engineering has emerged as a promising field for the regeneration and repair of damaged tissues and organs by copying the architectural and functional features of native ECM. However, traditional tissue engineering approaches have limitations in mimicking the complex electrical properties of native ECM and tissues. Conductive nanocomposites offer an innovative solution to this challenge by combining conductive nanoparticles with biocompatible matrices to create a conducive microenvironment for cell growth and tissue regeneration [4]. The conductive properties of these

nanocomposites facilitate better cell adhesion to the scaffold material [5]. Conductive nanocomposites can be used to deliver electrical stimulation to cells and tissues, which can promote cell proliferation, migration, and differentiation [4,5]. Electrical stimulation has been shown to accelerate tissue regeneration and improve the functionality of engineered tissues [5,6].

Therefore, conductive nanocomposites have emerged as a promising class of materials for tissue engineering particularly for neural tissue engineering [7,8], cardiac tissue engineering [4,8,9], bone tissue engineering [10–12], cartilage tissue engineering [13–15], and skin tissue engineering [16,17]. They can be used to create neural scaffolds that support the growth and differentiation of neurons [7]. Electrical stimulation provided by the nanocomposite can also facilitate neural network formation and functional integration with host tissues [8]. In cardiac tissue engineering, conductive nanocomposites can be used to create scaffolds for heart muscle regeneration [8]. Electrical stimulation can help promote cardiomyocyte alignment and contractile behavior, leading to improved tissue functionality [9]. In bone tissue engineering, conductive nanocomposites can be integrated into scaffolds to support the growth and differentiation of bone-forming cells (osteoblasts) [10]. Electrical stimulation can also promote bone mineralization and enhance the overall healing process [11]. In addition to scaffolds, conductive nanocomposites can also be used as bioelectrodes for electrical stimulation applications as well as biosensors [18,19].

However, it's essential to choose appropriate conductive nanomaterials and matrix materials that are biocompatible, non-toxic, and stable to create effective tissue engineering platforms [4]. Additionally, the mechanical properties and degradation rates of the nanocomposites should be tailored to match the specific tissue engineering application [4]. It has been shown that conducting polymers such as polyaniline and polypyrrole, can stimulate the attachment and proliferation of a variety of mammalian cell lines, including myoblasts, fibroblasts, and endothelial cells; however, these conducting polymers fail to mimic physiological moduli of ECM of various tissues [20]. That's why, incorporation of conductive nanomaterials including metallic, inorganic, organic or polymeric nanomaterials into a suitable biopolymer matrix, which can mimic a wide range of native ECM properties, has become an alternative strategy to create multifunctional scaffolds that provide the appropriate structural, mechanical, electrical, and biological properties to foster healthy cell function and tissue formation [21,22].

Noteworthy, there is a wide variety of carbon-based nanomaterials, such as carbon nanotubes, nanodiamonds, graphene oxide, and reduced graphene oxide can be used to develop electroconductive nanocomposite hydrogels [23–26]. However, compared to above mentioned carbon-based nanomaterials, nanosized carbon black (CB) is an ill-explored nanofiller for biomedical application [27]. As a sensing conductive filler, CB has a low cost, low density, and excellent intrinsic conductivity [28]. A CB filled polymer composite has many advantages, including easy fabrication and superior environmental stability [28]. The electrical conductivity of CB is influenced by its particle size, aggregate shape and structure, porosity, and surface chemistry. The electrical conductivity of carbon black/polymer mixtures depends also on polymer characteristics such as chemical structure, porosity and processing conditions. Improved conductivity of polymer/carbon black mixtures is achieved by using CB of smaller particle size (larger surface area), lower particle density (higher particle porosity), and higher structure (better aggregation).

Here, we present a series of nanocomposite hydrogels, which are composed of CB nanoparticles homogeneously dispersed into a gelatin-based hydrogel system. In tissue engineering, gelatin (G), a denatured collagen product, is widely used because the material is biocompatible, biodegradable, inexpensive, and easy to use [29]. However, G alone is structurally and mechanically weak and dissolves at physiological environment which limit its application as a scaffold material in tissue engineering [29,30]. To overcome these limitations, a mild crosslinking strategy is applied where G acts as a backbone polymer and poly(ethylene glycol)diglycidyl ether (PEGDGE) as the crosslink agent. By utilizing end epoxide groups, PEGDGE can react with multiple functional groups of G and acts as a spacer between two natural macromolecules, reducing steric hindrance and facilitating cell adhesion [31]. Chitosan (CH), a partially deacetylated derivative of chitin, is used to further enhance the biomimetic properties of the hydrogel. Most importantly, in the context of tissue engineering, CH

 doi:10.20944/preprints202308.1671.v1

is structurally similar to native ECM that facilitates cell-chitosan interaction [32]. Furthermore, CH possesses excellent biological properties such as biodegradability, anti-bacterial activity and biocompatibility [32]. To achieve anisotropic porous hydrogel, we employed unidirectional freezing technique using liquid nitrogen. We forced the degree of crosslinking through concerted effect of chemical reactions in solution and post curing treatment.

The overall aim and objective of this study is to develop gelatin-based conductive hydrogel scaffolds via a mild processing condition which includes aqueous media, various polymer assembly, crosslinking chemistry facilitating gelation with CB nanomaterial and to characterize structural property, mechanical property, thermal property, morphology, and electrical conductivity of the synthesized nanocomposite hydrogels to find their potential applications as tissue engineering scaffolds.

2. Materials and Methods

Materials

Type A gelatin (pharmaceutical grade, 280 bloom, viscosity 4.30 mPs), produced from pig skin, was purchased from ITALGELATINE, Italy). CH (molecular weight between 50000-190000 Da and degree of deacetylation 75-85%) was obtained from Fluka, Italy. PEGDGE (molecular weight 526 Da) was supplied by Sigma-Aldrich Co (Milan, Italy). Conductive nanosized carbon black (Printex XE2B) was purchased from Degussa Huls Chemicals S.p.A. and had an average particle size of 30 nm and BET surface area of 1000 m^2/g. Ethylene diamine (EDA) and acetic acid were provided by Fluka, Italy.

Methods

2.1. Synthesis of G/PEG/CH (CB) nanocomposite hydrogels

The G/PEG/CH (CB) nanocomposite hydrogel was prepared in different CB compositions, to be specific 10 %, 15 % and 20 % of CB, following a slightly modified method mentioned elsewhere [29]. For preparing G/PEG/CH (CB) nanocomposites with 10 % CB, an amount of 0.80 g pulverized CB was dissolved in 60 ml water and treated with magnetic stirring and ultrasonication until dispersed completely. Then gelatin granules (5.90 g) were added into CB solution and magnetically stirred for 2 h at 45 ^oC to homogeneously dissolve the gelatin. After that, PEGDGE (1.4 g) was introduced into the mixture followed by EDA (70 mg) under continuous magnetic stirring at 45 ^oC. Chitosan solution of 2 wt% was prepared by dissolving 0.7g CH in 1% aqueous acetic acid solution (35 g) and subsequently stirring for overnight. Then the previously prepared chitosan solution (33 g) was added into gelatin-PEG-CB reaction mixture and continued stirring for another 1 h (and 5 min sonication after an interval of 20 min magnetic stirring) under same temperature to obtain homogeneous reaction mixture. Finally, the reaction mixture was poured into plastic box, cooled to room temperature to form gel, frozen with liquid nitrogen, lyophilized, and post cured at 45 ^oC for 2 h. The same sequences were applied for fabricating G/PEG/CH (CB) nanocomposites with 15 and 20 % CB with the required amount of CB for each formulation. Three different G/PEG/CH (CB) nanocomposites were prepared, and the formulations were tabulated in **Table 1**.

2.2. Density and porosity measurement

The ethanol displacement method was used to measure the apparent density and porosity of the dry gel by soaking the pre-massed sample in a defined ethanol volume. The sample was previously placed under vacuum to remove the entrapped air, and the mass of the dry gel (W) was measured. Later, the sample was immersed into a graded cylinder containing a known volume (V_1) of ethanol, and total volume (V_2) of ethanol and gel was recorded. The gel was carefully removed from the ethanol 5 h later, and the residual volume (V_3) of the ethanol was measured. Finally, the total volume of gel was calculated as $V = V_2 - V_3$.

The apparent density (ρ) of hydrogel was calculated using the following equation:

$$\rho = W / V_2 - V_3$$

The porosity (ϵ) of hydrogel was measured by using the following equation:

 doi:10.20944/preprints202308.1671.v1

$$\epsilon = V_1 - V_3 / V_2 - V_3$$

2.3. Swelling ratio (%) measurement

The swelling ratio of the hydrogel was estimated by soaking the previously weighed dry sample in the distilled water in a thermostatic bath at the temperature of 37 °C. At predetermined time intervals, the sample was removed from the distilled water, the excess surface water was removed by gently pressing it with absorbent paper, and the weight was measured accurately using an electronic analytical balance. The percentage swelling ratio (%) was determined as:

$$S_R (\%) = (W_s - W_d / W_d) * 100$$

where W_s and W_d indicate the wet and initial dry weight of the sample, respectively. Each experiment was done using five samples, and the average value was exposed with standard deviation.

2.4. Chemical Structure Analysis

The chemical characterization of nanocomposite hydrogels was performed using Fourier transform infrared (FTIR) spectroscopy on dry hydrogels using a Thermo Scientific, Nicolet iS50 FTIR spectrophotometer equipped with a PIKE MIRacle attenuated total reflectance attachment and recorded over a range of 400 to 4000 cm^{-1} at a resolution of 4 cm^{-1}.

2.5. Thermogravimetric analysis

The exact amounts of CB in the nanocomposite hydrogels were evaluated by thermogravimetric analysis (TGA) run by a TGA 500 equipped using Hi-Res-Dynamic method with a Mettler TG50 microbalance heating a sample of about 5 mg into alumina crucible from room temperature to 700 °C at 50 °C/min under nitrogen flow (40 mL/min).

2.6. Morphology analysis

The morphology of the nanocomposite hydrogels was analyzed using a stereomicroscope (LEICA DMS 300) with reflected light. The dried samples were cut in the parallel (direction of ice crystal growth) and perpendicular direction to the macroporous channels, and the morphologies of the surfaces and textures were observed using the stereomicroscope.

2.7. Compression and cyclic compression tests

The mechanical properties of the nanocomposite hydrogels were measured using a universal testing system (INSTRON series 3366) equipped with a 50N load cell, in unconfined compression mode between two impermeable parallel plates. Specimens were cut from the sample bars into cuboid shaped samples using a precision rotary saw. Before the tests, the as-prepared samples were soaked in distilled water at 37 °C for 2 h. The actual height (H), width (W) and thickness (T) of the specimens were measured using an optical travelling microscope. Prior to initiating the compression test, a pre-load of 0.005N was applied in order to reduce the influence of surface artifacts. For compression test, cuboid-shaped samples were compressed at a strain rate of 10 mm/min up to maximum 50 % strain of the original heights, either along the parallel or perpendicular direction to the macroporous channels. The cyclic consecutive loading-unloading test was performed continuously for 10 cycles, as long as no significant change in curve shape was observed. At least three specimens were tested for each direction. For unconfined compression testing, the load–displacement (F–x) data are converted to stress–strain ($\sigma - \varepsilon$) data through simple geometrical relationships. Engineering stress was calculated by dividing the recorded force by the initial cross-section area. Engineering strain under compression was defined as the change in height relative to the original height of the individual specimen. The initial elastic modulus (stiffness) was calculated from the first compression cycle and determined as the linear segment slope of the compressive stress-strain within the range of 5-10 % strain. Compressive strength was defined as the maximum stress at 50 % strain.

Preprints (www.preprints.org) | NOT PEER-REVIEWED | Posted: 23 August 2023 doi:10.20944/preprints202308.1671.v1

The successive cyclic compression experiment involves loading-unloading pattern to reach different maximum strain (%) at each cycle. The specimen was first compressed (loaded) to a maximum strain of 20 % and then relaxed (unloaded). Sequentially, the specimen was compressed to 30 % maximum strain and relaxed again, repeating the operation increasing maximum strain to 40 % 50 % and 60 %. The energy absorbed by the nanocomposite hydrogels was calculated by the cyclic compression stress-deformation curves. The total energy applied to the hydrogel during the loading, defined as compression energy (kJ/m^3), was derived from the area included by loading curve and horizontal axis, while the energy released by the hydrogel during the unloading, defined as relaxation energy (kJ/m^3), is the area bounded between unloading curve and horizontal axis. Hysteresis loop area indicates the dissipated energy due to the viscous nature of the hydrogels, so the dissipation energy (kJ/m^3) loss during hysteresis cycle was calculated as the difference between the area under the load curve (compression energy) and the discharge (relaxation energy) curve from the stress-deformation curve. The percentage of dissipation energy (%) was determined by dividing the dissipation energy by compression energy. The same computations were performed for cyclic compression test with gradually increasing maximum compressive strain from 20 % to 60 %, calculating the dissipation energy (kJ/m^3) and percentage dissipation energy (%) at each maximum strain.

2.8. Electrical impedance measurement

Preliminary electrical impedance analysis was carried out considering alternate current (AC) regimen, in the frequency range of 10^2-10^6 Hz at room temperature by using a commercial impedance analyzer (HP4194A). Nanocomposite hydrogels filled with different weight percentages of carbon black nanoparticles were tested in both dry and hydrated state. In order to highlight the resistive and capacitive behavior, complex impedance associated to the samples was studied in term of modulus and phase. Tests were performed in triplicate.

3. Results

3.1. Preparation of G/PEG/CH (CB) nanocomposite hydrogels and their physical properties

Conductive nanocomposites have emerged as promising materials in the field of tissue engineering due to their unique properties that can enhance tissue regeneration and repair. These materials combine conductive elements such as conductive nanoparticles or conductive polymers with biocompatible polymers, providing electrical conductivity while supporting cell growth and tissue integration. Motivated by this, we synthesized G/PEG/CH (CB) nanocomposites using a versatile approach consisted of liquid-phase pre-crosslinking/grafting, unidirectional freezing process carried out by liquid nitrogen subsequent freeze-drying, and post-curing process, as shown in **Figure 1**.

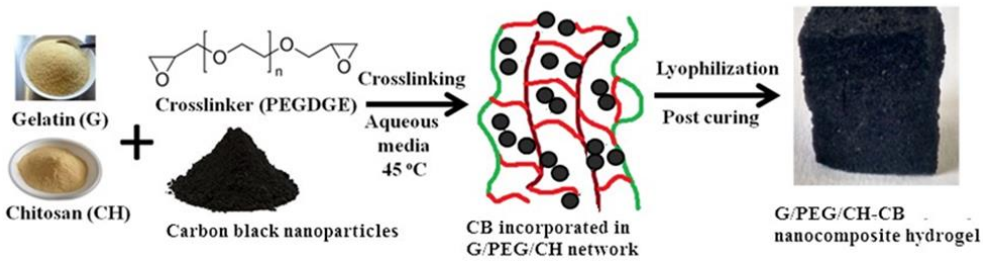

Figure 1. Schematic diagram illustrating synthesis process of nanocomposite hydrogels.

The composition of the G/PEG/CH (CB) nanocomposite hydrogels are presented in **Table 1**. We calculated the exact amount of CB present in the final nanocomposite hydrogels with the help of TGA analysis (**Figure 2a**) and the results are illustrated in **Table 1**. TGA was performed with a heating rate of 50 °C/min to 700 °C under nitrogen atmosphere. Under this operating condition, pristine conductive carbon black showed no weight loss indicating indifferent to thermal decomposition.

Preprints (www.preprints.org) | NOT PEER-REVIEWED | Posted: 23 August 2023 doi:10.20944/preprints202308.1671.v1

However, G/PEG/CH (control sample) hydrogel showed significant weight loss and retained 19.80 % of its original weight at the same condition. **Figure 2a** showed the increased percentage residue with the higher CB content in the sample, and we applied 'subtraction' approach to determine the final CB content assuming that increased percentage residue attributed to thermally resistant CB. We calculated final CB content in the nanocomposite hydrogel by subtracting the individual residue content to control one. Homogeneous dispersion of CB into polymeric network is important to avail the utmost beneficial contribution of CB incorporation. On visual inspection during synthesis, we could not observe any agglomeration of CB into polymeric system. Furthermore, to confirm the uniform dispersion, we carried out TGA analysis of G/PEG/CH (CB-1) nanocomposite using different sections of the same sample, namely, top, middle, and bottom parts. **Figure 2b** exhibits no difference in residue for all sections confirming uniform CB dispersion into nanocomposite hydrogels.

Table 1. Composition, density and porosity of the G/PEG/CH (control sample) and G/PEG/CH (CB) nanocomposite hydrogels.

	Composition (w/w %)					Physical properties	
Hydrogels	**G**	**PEG**	**CH**	**CB***	**CBΦ**	**Apparent density (g/cm³)**	**Porosity (%)**
G/PEG/CH	74	18	8	-	-	0.11 ± 0.03	77 ± 2.0
G/PEG/CH (CB 1)	67	16	7	10	6.95	0.12 ± 0.03	65 ± 10
G/PEG/CH (CB 2)	63	15	7	15	13.6	0.13 ± 0.01	64 ± 3.0
G/PEG/CH (CB 3)	60	14	6	20	18.2	0.13 ± 0.01	59 ± 10

*denotes initial CB content and Φ denotes CB content in the final product after washing and calculated by TGA analysis.

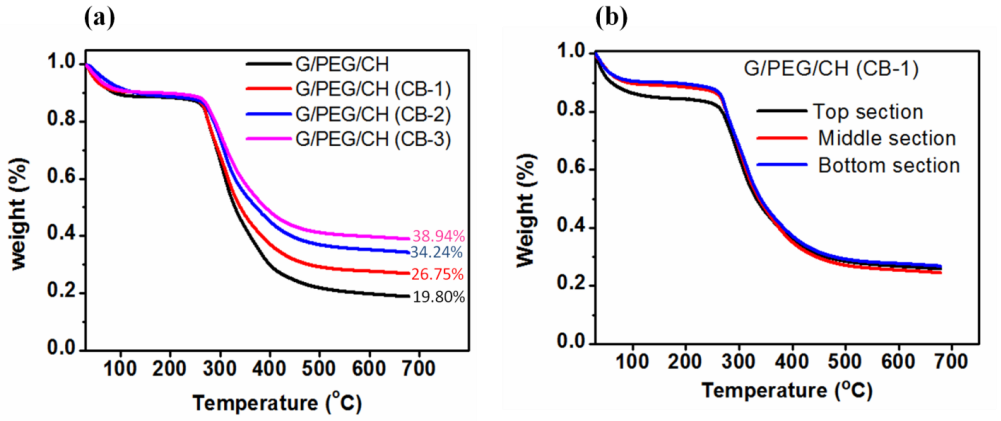

Figure 2. TGA curves of control G/PEG/CH and G/PEG/CH (CB) nanocomposite hydrogels. **(a)** Thermograms showing the residue at 700 °C under nitrogen atmosphere with a purge rate of 50 mL/min and **(b)** showing the trend of weight loss and residue of different layers of same G/PEG/CH (CB-1) nanocomposite hydrogel.

3.2. Chemical structure characterization

The chemical structure (functional groups) of the nanocomposite hydrogels was analyzed by FTIR using the washed samples, and **Figure 3** displays the IR spectrum of control and nanocomposite hydrogels. The physico-mechanical properties of the nanocomposite hydrogels depend on the molecular level interaction of G-CB, CH-CB and PEG-CB. Gelatin showed prominent amine peaks around 1540 cm^{-1} (due to -NH bending vibrations and C-N stretching vibrations) and 1650 cm^{-1} (due to C=O stretching vibrations) [29]. The representative intense peak presented around 1096 cm^{-1}, which is assigned to C-O stretching (ether bond C-O-C), validated the presence of PEG in the final

Preprints (www.preprints.org) | NOT PEER-REVIEWED | Posted: 23 August 2023 doi:10.20944/preprints202308.1671.v1

hydrogels. Addition of CB neither split nor shift any peaks or not induce new peaks, indicating no chemical interaction with polymers at molecular level.

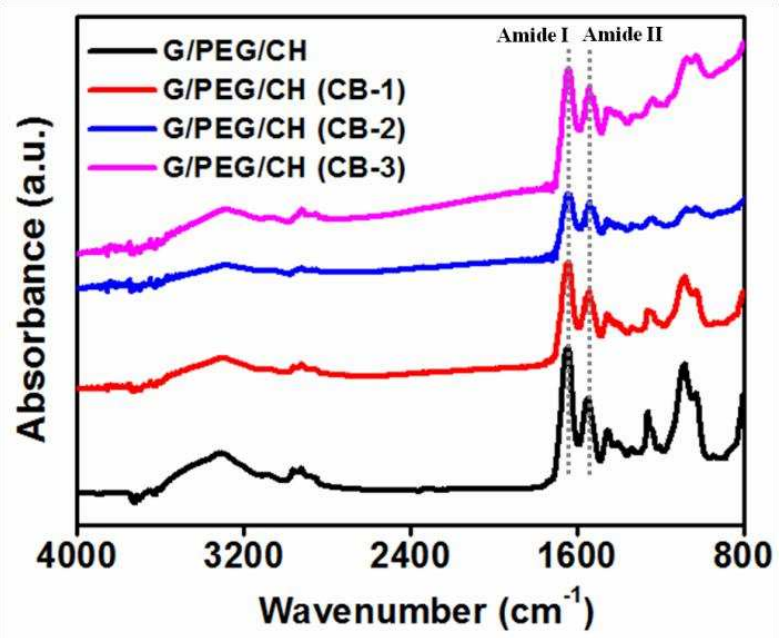

Figure 3. FTIR spectra of control G/PEG/CH and G/PEG/CH (CB) nanocomposite hydrogels.

3.3. Apparent density, porosity and swelling ratio

The apparent density and total average porosity of the nanocomposite hydrogels were investigated using ethanol displacement method and the results are shown in **Table 1**. The apparent density of G/PEG/CH (CB) nanocomposite hydrogels showed higher values than that of the G/PEG/CH control sample. However, the different amount of CB in these hydrogels appeared to slightly influence the density among the nanocomposites, showing similar density values around 0.13 g/cm^3. At the same time, the decrease of hydrogel porosity was observed with the increase of nanofiller CB amount. The increasing of carbon black amount as filler actually decreased the porosity and favored the formation of hydrogel with a wider distribution of micropores. The control G/PEG/CH hydrogel showed a percentage porosity of 77 %, whereas the G/PEG/CH (CB) nanocomposite hydrogels showed an average percentage porosity of 62.66 %. We also investigated the effect of CB incorporation on the swelling ratio of the nanocomposite hydrogels. As shown in **Figure 4**, the swelling ratio of nanocomposites did not seem to be significantly influenced by the addition of CB. All nanocomposite hydrogels showed a higher swelling ratio (~ 730 %) suitable for tissue engineering applications.

Preprints (www.preprints.org) | NOT PEER-REVIEWED | Posted: 23 August 2023 doi:10.20944/preprints202308.1671.v1

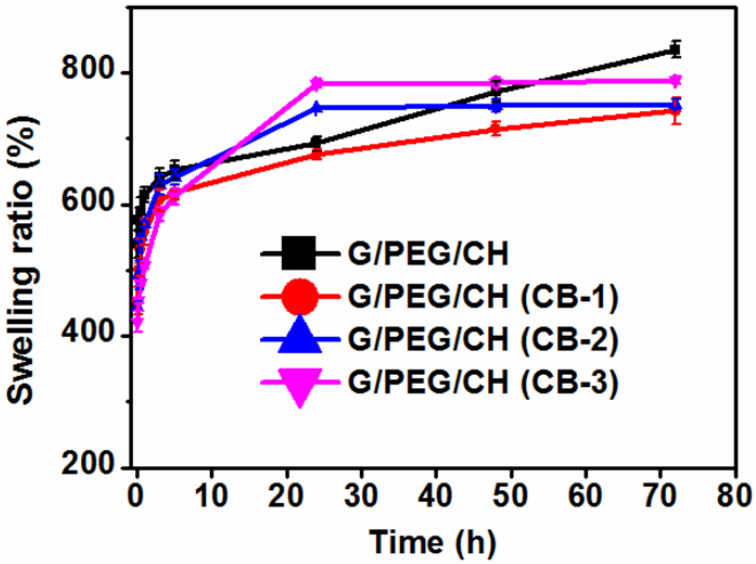

Figure 4. Swelling ratio of control G/PEG/CH and G/PEG/CH (CB) nanocomposite hydrogels.

3.4. Morphological evaluation

Scaffolds for tissue engineering applications should have an interconnected porous structure for cell infiltration and effective transport of nutrients and oxygen. Freeze drying technique produced thin skin with dense texture (**Figure 5a,b**). However, beneath the skin the hydrogel was highly porous (**Figure 5c,d**). A closer examination revealed this skin was composed of micropores (inset). However, removing skin disclosed interconnected macropores of thin walls which themselves composed of micropores (**Figure 5c,d**). Overall, freeze drying technique used in our protocol produced highly porous hydrogels below a thin skin with dense texture.

We also investigated the effect of CB incorporation into pore morphology, and we analyzed the pore morphology in the parallel (side view) and perpendicular (cross section view) to direction of ice crystal growth as shown in **Figure 6(a–f)**. With 10% CB content, the hydrogel showed anisotropic pore morphology: larger macroporous channels and random pores formation along and normal to the ice crystal growth, respectively (**Figure 6a,c**). Surprisingly, higher CB content compromised with anisotropic nature of the hydrogels as well as pore sizes. The cross-section view of the G/PEG/CH (CB-2) hydrogel revealed denser texture with smaller sizes of pores (**Figure 6b**). Smaller channels, both in length and diameter, were observed with a 15 % CB content along the direction of ice crystal growth (white color arrows indicate the smaller channels (**Figure 6e**). Further increment of CB concentration to 20 % (G/PEG/CH (CB-2)), imparted more compact structures in both directions; completely nullifying the anisotropic pore morphology and introducing isotropic structure (**Figure 6e**). Excitingly, this CB concentration-imposed pore morphology triggered mechanical response accordingly (discussed below). The most plausible explanation behind the transition of anisotropic to isotropic pore morphology with the increased CB content might be the higher CB concentration restricted the directional ice crystal growth.

Preprints (www.preprints.org) | NOT PEER-REVIEWED | Posted: 23 August 2023 doi:10.20944/preprints202308.1671.v1

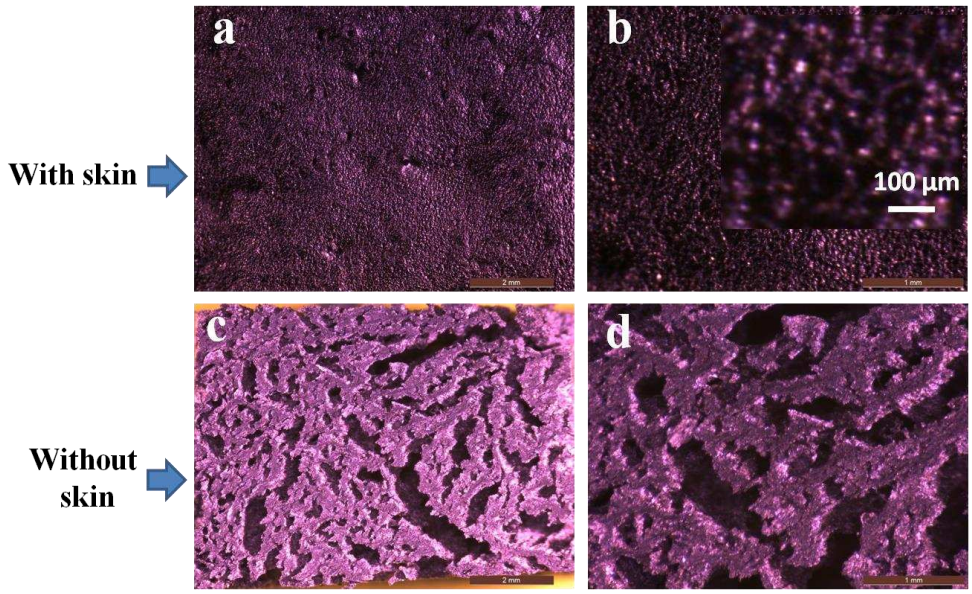

Figure 5. Optical microscopic visualization of nanocomposite hydrogels. **(a, b)** with skin (inset shows magnification with scale bar 100 µm and dark parts resemble the pores) and **(c, d)** without skin.

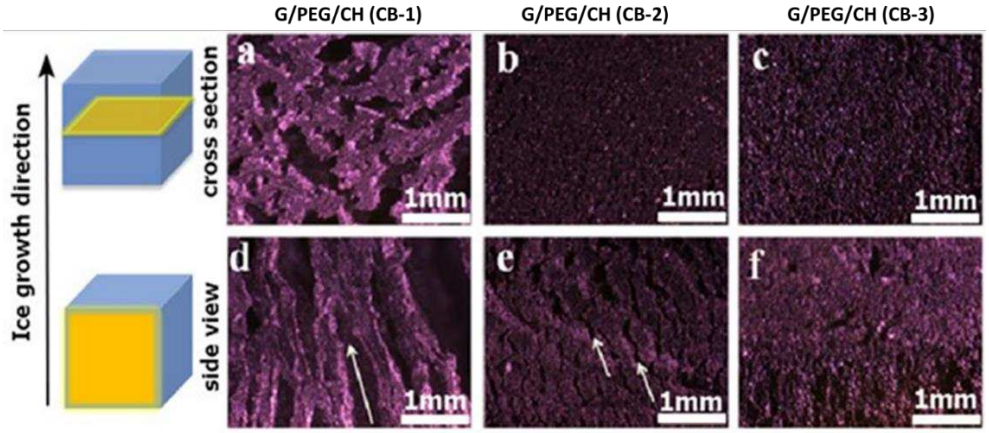

Figure 6. Optical images displaying the cross section and side view of the nanocomposite hydrogels for (**a, d**) G/PEG/CH (CB-1), (**b, e**) G/PEG/CH (CB-2) and (**c, f**) G/PEG/CH (CB-3). The arrows indicate the macroporous channeling. Scale bars are 1mm (a-f).

3.5. Compressive mechanical properties

To explore the effect of CB incorporation on the mechanical properties, uniaxial unconfined compression test was done on swollen samples in distilled water at 50 % strain (**Figure 7**). It was obvious from **Figure 7** that the nanocomposite hydrogels showed reversible behavior (returned to original position) during compression test. The initial elastic modulus (stiffness) was calculated from the initial linear regions of the stress-strain curves (3 to 10 % strain) and the stress at 50 % strain was considered at strength. All the hydrogels were compressed in two directions (parallel and perpendicular) to examine the effect of pore morphology on the mechanical stiffness and strength, and the average values of results were summarized in **Table 2**. **Figure 8a–c** shows the stress-strain curves of nanocompostie hydrogels obtained from mechanical data when samples were subjected to compression both in parallel and perpendicular direction to the ice crystal growth. It was noticed that the anisotropic mechanical phenomenon became negligible increasing the CB amount in the nanocompostie hydrogels. Clearly, G/PEG/CH (CB-1) nanocomposite hydrogel showed a significant anisotropic mechanical property displaying an anisotropic ratio - ratio of modulus on parallel direction to perpendicular direction - of 3.70 **(Figure 8a**). Noteworthy, anisotropic mechanical

Preprints (www.preprints.org) | NOT PEER-REVIEWED | Posted: 23 August 2023 doi:10.20944/preprints202308.1671.v1

response significantly reduced with 15 % CB content (G/PEG/CH (CB-2), **Figure 8b**) while as, completely diminished with 20 % CB content (G/PEG/CH (CB-3), **Figure 8c**). The pore morphology of the nanocomposite hydrogels imparted these direction-dependent mechanical responses. Notably, G/PEG/CH (CB-1) nanocomposite hydrogel showed around a four-fold (0.063 MPa to 0.230 MPa) increase in stiffness when compress in parallel direction to macropore channels compared to perpendicular direction (**Table 2**). The two best plausible explanations for the increased stiffness when compressed in parallel direction in contrast to perpendicular compression for G/PEG/CH (CB-1) nanocomposite hydrogel might be due to: (i) the large lamellae which act as pillars reinforcing the hydrogel and (ii) the presence of more entrapped pressurized water between two compressive plates so that water could not be easily squeezed out [29].

The direction-dependent stiffness of anisotropic hydrogel was correlated with their anisotropic pore structures. As a possible confirmation of this, we could notice that a greater extent of macroporous channels along the direction of freezing in G/PEG/CH (CB-1) nanocomposite hydrogel made it an anisotropic hydrogel. On the other hand, a dimensional reduction of the walls of macrochannels in the hydrogel with 15 % of CB corresponded to a loss of the anisotropic behaviour. In G/PEG/CH (CB-2) nanocomposite hydrogel, the difference between directional-dependent stiffness and strength was so little that we could treat it as an intermediate hydrogel in terms of mechanical anisotropy. The typical channel-like morphology disappeared in G/PEG/CH (CB-3) nanocomposite hydrogel, and the more compact pore structure probably allowed the water to squeeze out in a similar way in both directions making it a perfectly isotropic hydrogel. **Figure 9** demonstrates the trend of compressive stiffness and strength variation with CB content. **Figure 9** and **Table 2** showed a significant improvement of stiffness and strength upon addition of CB into hydrogel system. For example, three-fold increase in both stiffness and strength was observed with 20 % CB content. However, nanocomposite hydrogel containing 10 % CB displayed similar stiffness and strength values of G/PEG/CH alone in both directions.

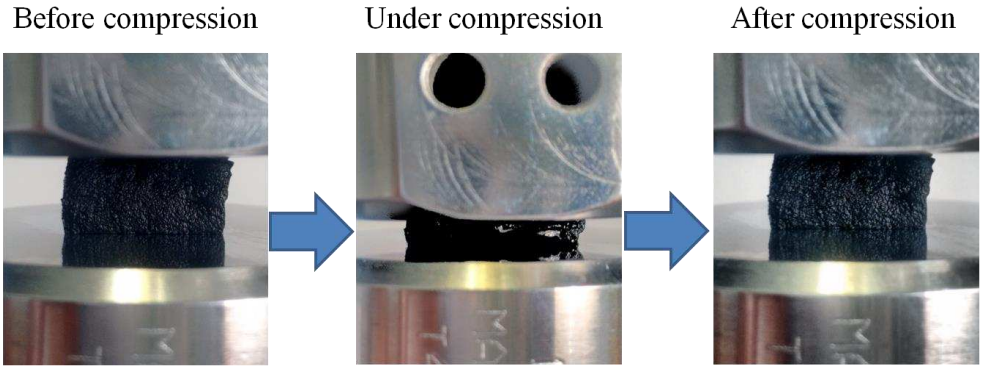

Figure 7. Optical images showing the compression test up to 50 % strain and mechanical reversibility after deformation.

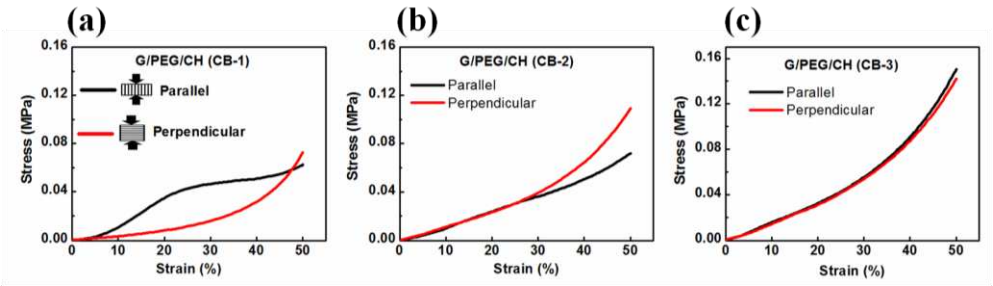

Figure 8. Stress-strain curves obtained from compression tests of fully swollen nanocomposite hydrogels. (**a**) G/PEG/CH (CB-1), (**b**) G/PEG/CH (CB-2) and (**c**) G/PEG/CH (CB-3).

Table 2. Compressive mechanical properties of G/PEG/CH control and nanocomposite hydrogels.

Preprints (www.preprints.org) | NOT PEER-REVIEWED | Posted: 23 August 2023 doi:10.20944/preprints202308.1671.v1

Sample name	Modulus (MPa)	Stress (MPa) at 50% strain	Compression direction	Pore morphology
G/PEG/CH	0.247 ± 0.03	0.0462 ± 0.01	Parallel to smaller macropore channels	Anisotropic
G/PEG/CH	0.042 ± 0.01	0.0534 ± 0.01	Perpendicular to smaller macropore channels	
G/PEG/CH (CB-1)	0.230 ± 0.05	0.053 ± 0.01	Parallel to smaller macropore channels	Anisotropic
G/PEG/CH (CB-1)	0.063 ± 0.02	0.057 ± 0.02	Perpendicular to smaller macropore channels	
G/PEG/CH (CB-2)	0.128 ± 0.01	0.132 ± 0.03	Parallel to smaller macropore channels	Intermediate behaviour
G/PEG/CH (CB-2)	0.112 ± 0.01	0.106 ± 0.04	Perpendicular to smaller macropore channels	
G/PEG/CH (CB-3)	0.173 ± 0.01	0.146 ± 0.01	No observable macropore channels	Isotropic

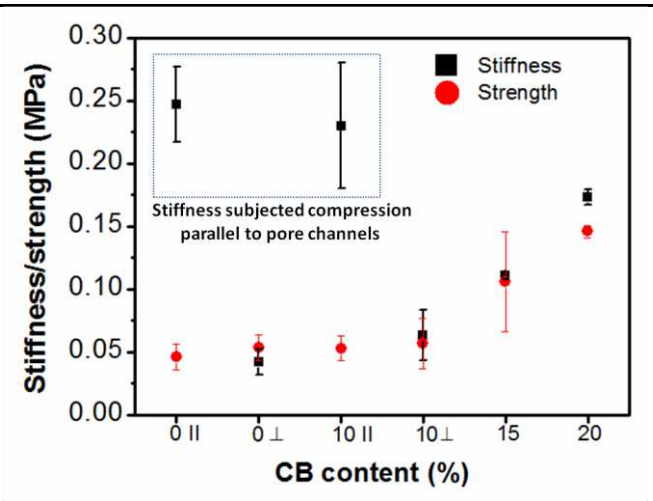

Figure 9. Stiffness and strength of the nanocomposite hydrogels as a function of CB content (∥ indicates compression parallel to smaller macropore channels and ⊥ indicates compression perpendicular to smaller macropore channels).

In addition to investigating the effect of CB content on the mechanical stability of the nanocomposite hydrogels, cyclic compression tests with ten loading-unloading cycles were also performed. **Figure 10** shows cyclic compressive stress-strain curves for up to 10 consecutive cycles at 50 % maximum strain without waiting time in parallel and perpendicular direction to the macroporous channels of the G/PEG/CH (CB-1) nanocomposite hydrogel in wet condition. **Figure 11** presents cyclic compressive stress-strain curves of G/PEG/CH (CB-2) and G/PEG/CH (CB-3) nanocomposite hydrogels as well as the corresponding stress-time curves.

As displayed by **Figure 10a**, the stress-strain curves of G/PEG/CH (CB-1) nanocomposite hydrogel clearly showed two different pathways during loading and unloading cycles, resulting in hysteresis loops. With regard to cyclic compression in a direction parallel to the macroporous channels, a pronounced deviation in stress-strain loading-unloading curves was shown between 1st and 2nd cycle, which indicated the occurring of irreversible damage during 1st cycle. It has been hypothesized that those smaller lamellae bridges connecting larger lamellae might be fractured

 doi:10.20944/preprints202308.1671.v1

during first cycle; furthermore, the characteristic plateau region was affected by these major micro fractures in the hydrogel involving a more collapsed structure and reduced buckling resistance of the lamellae for the consecutive cycles [29,30]. However, a slighter reduction in slope and maximal stress at 50 % strain was observed at each compressive cycle from 2nd to 5th consecutive loading-unloading cycles in the material, due to the occurring of other minor micro fractures. After 5th cycle, all following hysteresis loops were closely overlapped indicating that the hydrogel achieved a mechanically stable structure. It has been noticed that all unloading curves returned to 0 % strain, indicating full shape recovery of the hydrogels even at 50 % deformation. The stress responses (**Figure 10c**) of the G/PEG/CH (CB-1) nanocomposite hydrogel compressed at a constant strain level of 50 % was shown as a function of time during the 10 cycles. It was observed that the induced stress exhibited a transition phenomenon: during 1st cycle the induced stress was 0.064 MPa but, during subsequent cycles, it was gradually decreased and became stationary, reaching a constant value of 0.056 MPa after multiple cycles. This mechanical response is the outcome of a stress softening tendency described as Mullins' effect, which is characterized by a lower resulting stress for the same applied strain. It is often reported in filled and non-filled rubber-like materials, and such behaviour is known as "preconditioning" [33].

Figure 10b shows the stress-strain curves resulting from the cyclic loading unloading curves compressed perpendicular direction to the macroporous channels. In this case, stress-strain curves represented very small variation between 1st and 2nd cycle curves, indicating some minor irreversible micro fractures during 1st loading. However, 2nd cycle, and all sequent hysteresis loops were overlapped suggesting that the hydrogel had a good reversible behaviour. The corresponding stress-time plot (**Figure 10d**) also confirmed the mechanical stability. The maximal stress slightly reduced during the 2nd cycle, however, rapidly reached a stationary value after subsequent cycle. The mechanical responses observed by G/PEG/CH (CB-2) and G/PEG/CH (CB-3) nanocomposite hydrogels during compression testing (**Figure 11**) were similar. During the 1st loading some sorts of micro fracture occurred, however, 2nd cycle on, and subsequent cycles nearly identical hysteresis loops were observed. They exhibited a preconditioning behaviour up to the 5th cycle, as result of stress softening effect just explained in the previous paragraph.

Cyclic stress softening can be characterized by the amplitude of normalized stress decrease and by the number of cycles needed to reach a stabilized state. This effect was also evaluated by calculating the ratio of the maximum stress of every cycle to maximum stress of the first cycle (normalized stress). As observed in **Figure 12**, the normalized stress over 10 cycles preserved at least 85 % of the maximal stress reached in the first cycle for G/PEG/CH (CB-1) in parallel direction, G/PEG/CH (CB-2) and G/PEG/CH (CB-3). A lower stress softening was observed particularly for G/PEG/CH (CB-1) in perpendicular direction, showing an amplitude of normalized stress decrease of 5 %, confirming what discussed above.

In summary, during the first cycles, the hydrogels showed a Mullins effect, with the reduction of stiffness and stress at every cycle. After few cycles, the material behaviour was stabilized, and the hydrogels were able to sustain a compressive strain of 50 % with full strain recovery. All the nanocomposite hydrogels maintained their original shape and their load bearing capability up to such a high level of deformation. It might be possible that many microscopic flaws were created within the hydrogels, but no macroscopic cracks propagated; as a result, the hydrogels were not fractured at a macroscopic level.

Preprints (www.preprints.org) | NOT PEER-REVIEWED | Posted: 23 August 2023 doi:10.20944/preprints202308.1671.v1

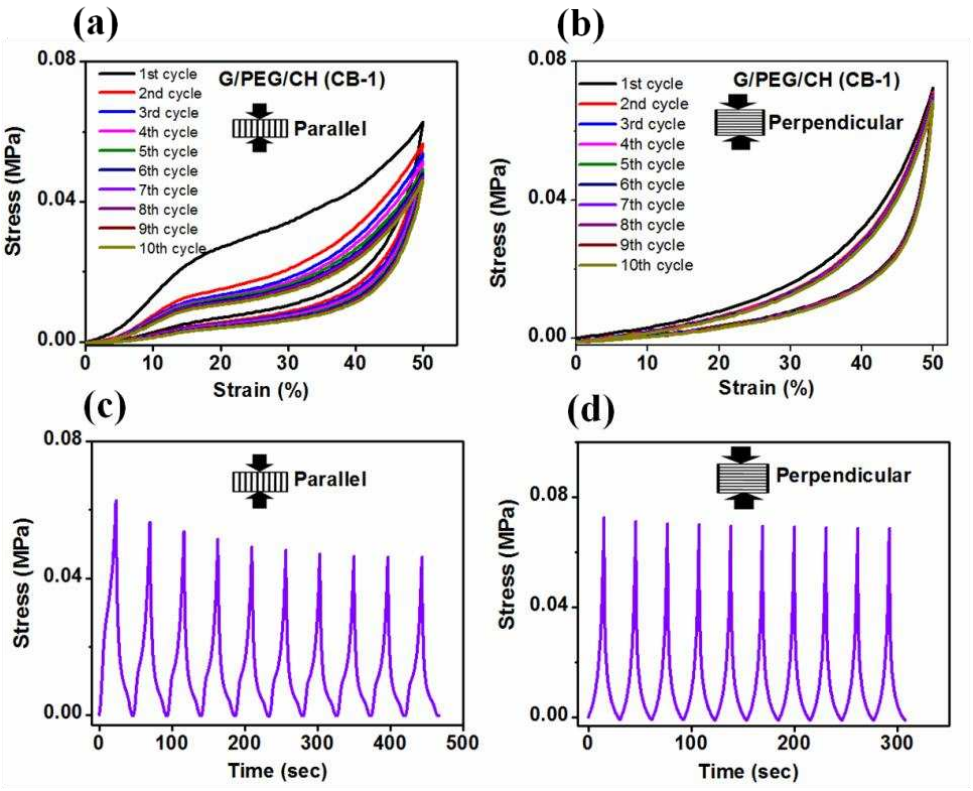

Figure 10. Cyclic compressive stress-strain curves of G/PEG/CH (CB-1) nanocomposite hydrogel for up to 10 consecutive cycles at 50 % maximum strain along (**a**) parallel and (**b**) perpendicular direction to the macroporous channels. Corresponding stress-time curves in (**c**) parallel, and (**d**) perpendicular direction.

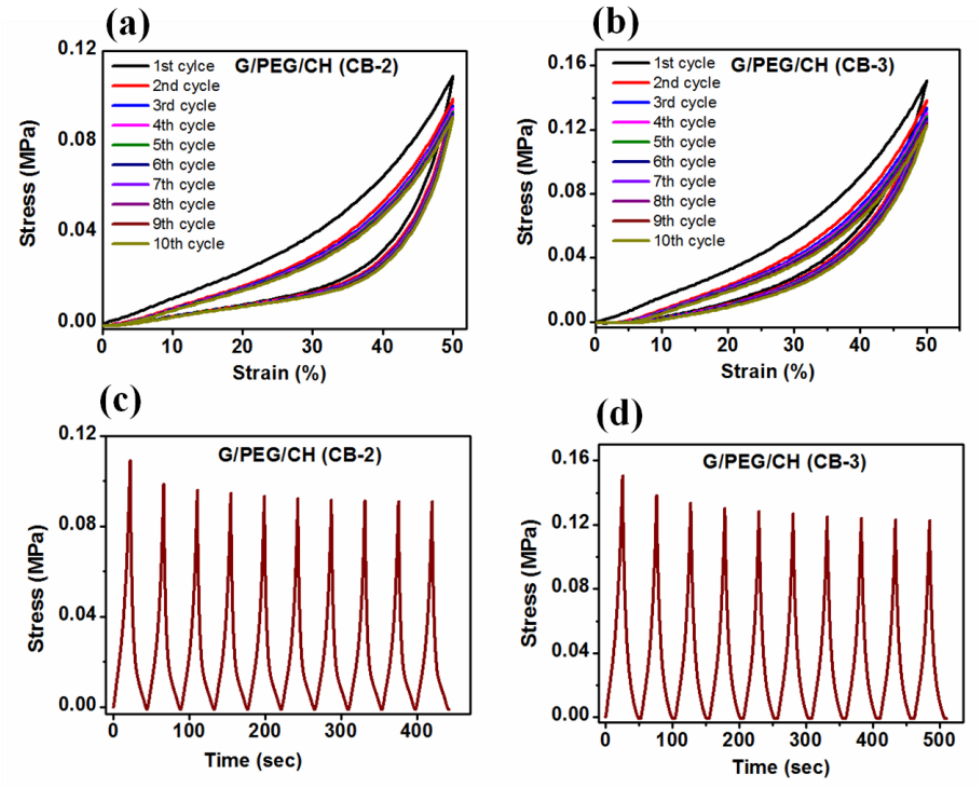

Figure 11. Cyclic compressive stress-strain curves of hydrogels for up to 10 consecutive cycles at 50 % maximum strain without waiting time. **(a)** G/PEG/CH (CB-2) **(b)** G/PEG/CH (CB-3); and **(c)** and **(d)** corresponding stress-time curves, respectively.

Preprints (www.preprints.org) | NOT PEER-REVIEWED | Posted: 23 August 2023 doi:10.20944/preprints202308.1671.v1

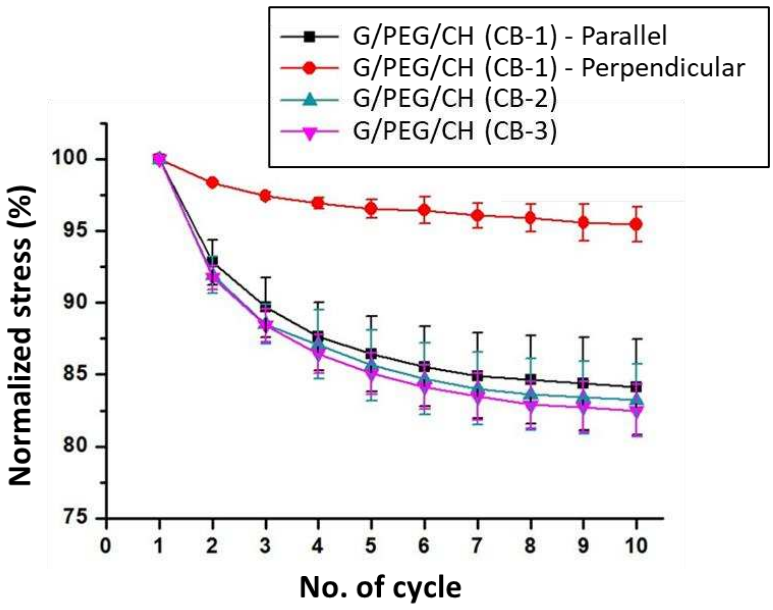

Figure 12. Amplitude of normalized stress decreases over the ten consecutive compressive cycle of the nanocomposite hydrogels. Normalized stress was defined as the ratio of observed stress at each cycle to the maximum stress at 1st cycle.

Additionally, dissipation energy calculated for each cycle also showed sharply reduced absorbed energy after 1st cycle, but nearly constant for subsequent cycles (**Figure 13a**). In the case of G/PEG/CH (CB-1) nanocomposite hydrogel when compressed parallel to the macroporous channels, the calculated dissipation energy was double if compared to those of perpendicular direction (**Figure 13a**). Furthermore, the slope of this decreasing is more marked along the parallel direction before the tested samples reached a constant value after a few cycles for both compression directions. This might be explained by a more stable structure in perpendicular direction as depicted before. Additionally, as shown in **Figure 13b**, the percentage dissipated energy was the highest at 1st cycle for all hydrogels. However, the percentage of dissipation energy was found to be similar after 5th to subsequent 10th cycle further confirming the achieved mechanical stability after few cycles. Excitingly, all nanocomposite hydrogels maintained their original shapes after undergoing such a high level of deformation.

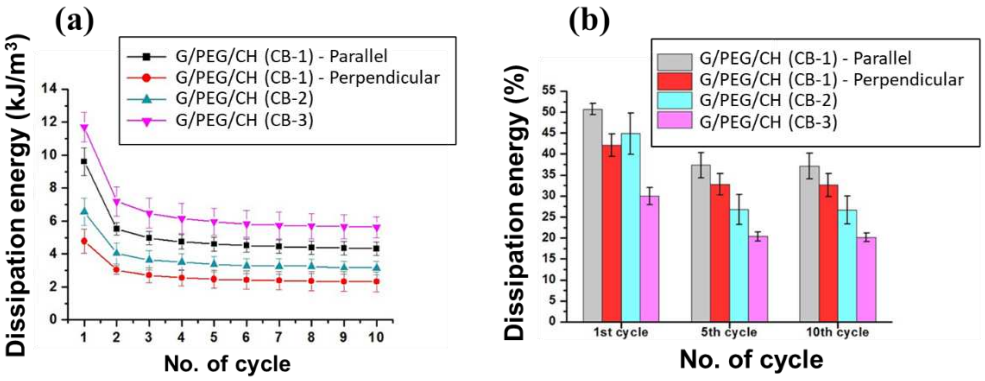

Figure 13. Energy dissipation of nanocomposite hydrogels subjected to compression consisting of ten loading-unloading cycles at 50 % strain. **(a)** Effect of number of cycles on energy dissipation and **(b)** calculated percentage energy dissipation at 1st, 5th and 10th cycles.

Moreover, nanocomposite hydrogels were subjected to cyclic compression with increasing maximum strain ranging from 20 to 6 0% and stress-strain curves were represented in **Figure 14a–d**. In addition, energy dissipation was calculated from the hysteresis loop with different strain levels (**Figure 15**). **Figures 14** and **15** highlighted that hysteresis became apparent above 30 % strains and

 doi:10.20944/preprints202308.1671.v1

sharply increased with increasing strain levels indicating increased absorption of energy during higher deformation. For all cases, the hysteresis loops area became larger with increasing maximum strain. Furthermore, as presented in **Figure 15a**, G/PEG/CH (CB-1) nanocomposite hydrogel showed exponentially increasing trend of dissipation energies with the increasing of maximum strain, suggesting capability of hydrogel to effectively dissipate energy at larger deformation, also indicating a gradual fracture process of the gel network while reaching higher deformation level respect to the previous cycle. The slightly higher dissipated energies for parallel compression of G/PEG/CH (CB-1) with respect to the perpendicular compression might be due to the migration of more pressurized water throughout the porous network. The exponential growth of dissipated energies at higher deformation levels became more apparent when the CB amount was increased to 15 % and 20 %, achieving values of 12 kJ/m^3 and 16 kJ/m^3 for 60 % strain, respectively, which are twice, and three times more than the energy dissipated at 10 % CB content.

Percentage dissipation energy is often used to quantify the energy dissipation ability of a tough hydrogel. Higher level of deformation involves more dissipation due to the more stress applied to the material (higher friction). Applying a greater force, a higher loading energy was conferred to the material and the dissipation energy increased for the water movement. As shown in **Figure 15b**, G/PEG/CH (CB-1) and G/PEG/CH (CB-2) nanocomposite hydrogels exhibited similar dissipated energy capacities, which increased slightly with higher deformations. At the same time, G/PEG/CH (CB-3) demonstrated lower dissipation ability, but still increased strain up to 60 %, suggesting a less pronounced bond rupture capacity, increased elastic properties, and more deformation tolerance. It is noteworthy that with 20 %CB the percentage dissipation energy is more constant, and it probably be able to sustain higher deformation that led to higher values of percentage dissipation energy (not necessarily linear increasing over 60% of deformation). This CB nanofiller reinforced the hydrogel by giving a greater effect on strength than modulus. This involved high compression energy during loading; as the deformation applied to the material increases, the dissipation energy increases but the compression energy increases relatively more (due to the reinforcement effect). These results clearly suggested that the nanocomposite hydrogel possessed CB concentration dependent and strain-dependent energy dissipation behaviour, and effective energy dissipation occurred at the higher strain deformation.

It is generally accepted that the stiffness and toughness of conventional materials are two opposite mechanical parameters. Interestingly, our G/PEG/CH (CB) nanocomposite hydrogel can simultaneously increase both stiffness and toughness with increasing CB concentration. This could be attributed to hybrid physical and chemical crosslinking in the nanocomposite hydrogel. The enhancement in the elastic modulus (indicator of the stiffness) of G/PEG/CH(CB) nanocomposite hydrogels is attributed to the increase in elastically effective G/PEG/CH chains and the reinforcing effect of the carbon black acting as a filler. The rupture (or peeling) of physically adsorbed G/PEG/CH chains from CB is accompanied by energy dissipation, which consequently improves the crack resistance of the hydrogels. In addition, as more G/PEG/CH chains are adsorbed on CB particles, more energy is dissipated. Therefore, the toughness of G/PEG/CH (CB) nanocomposite hydrogels continue to increase with CB concentration. Taken together, slight decrease of stress and returning and no residuary strain during the consecutive loading-unloading cycles demonstrated elasticity, excellent shape-recovery property and good mechanical stability of the nanocomposite hydrogels.

Preprints (www.preprints.org) | NOT PEER-REVIEWED | Posted: 23 August 2023 doi:10.20944/preprints202308.1671.v1

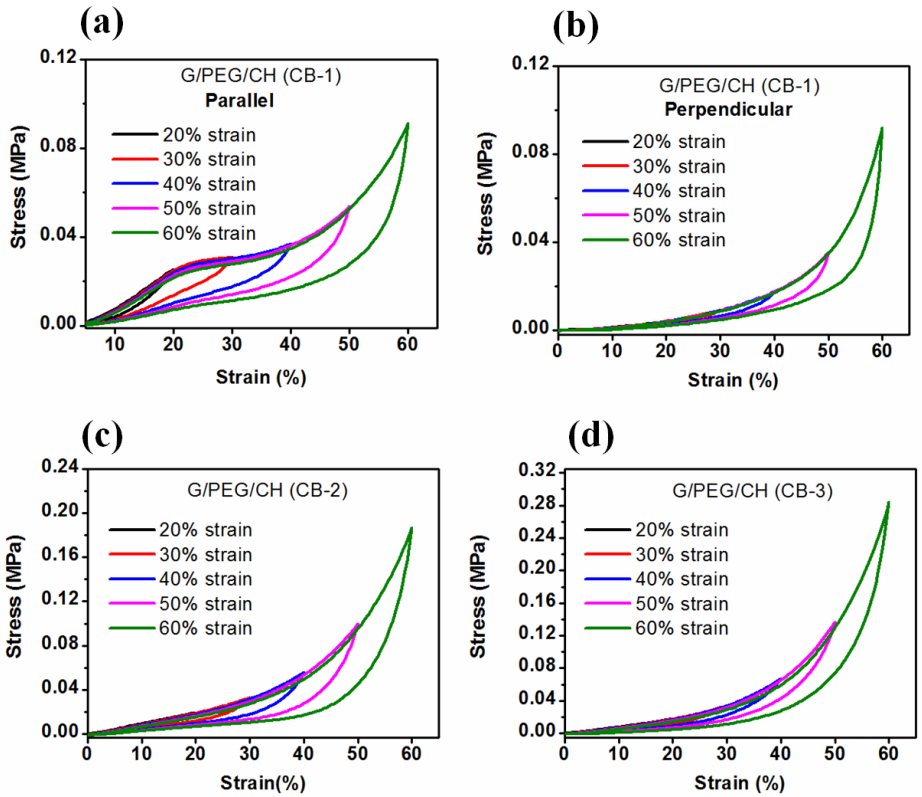

Figure 14. Stress-strain curves of cyclic compression test with amplitude ranging from 20 to 60 % strain applied to nanocomposite hydrogels, correspondingly for (**a**) G/PEG/CH (CB-1)-parallel, (b) (G/PEG/CH (CB-1)-perpendicular, (**c**) G/PEG/CH (CB-2) and (**d**) G/PEG/CH (CB-3). .

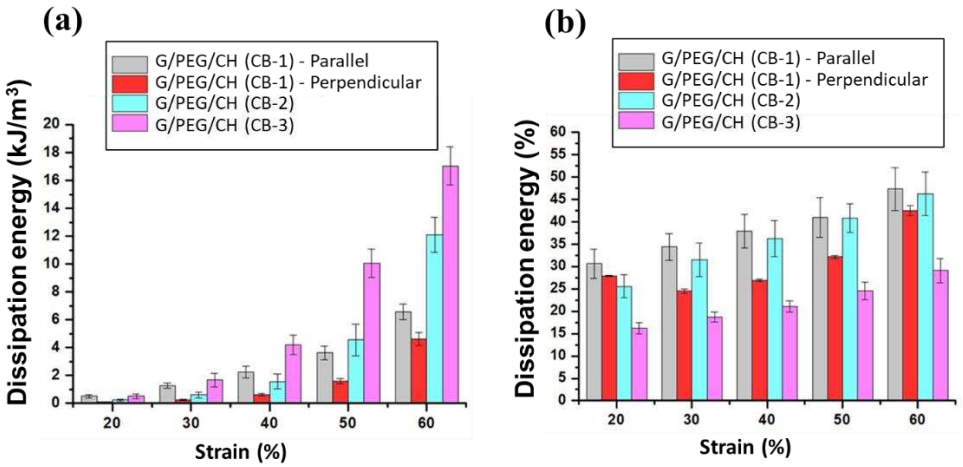

Figure 15. Energy dissipation calculated from the observed hysteresis during compressed at different strains. (**a**) The hysteresis energies of nanocomposite hydrogels compressed at different maximum strains and (**b**) the percentage dissipation energy for different CB concentrations.

3.6. Electrical impedance

To highlight the resistive and capacitive behavior, complex impedance associated to the samples was studied in terms of modulus and phase in dry and wet condition, as presented in **Figures 16** and **17,** respectively. Considering dry testing, the results reported good optimally tunable electrical properties with characteristic frequency of transition between resistive- and capacitive-like behaviors, depending on CB content, despite the presence of noise at low frequency. Such a result appears to be promising in view of the application of electrical stimuli, even compared with more

Preprints (www.preprints.org) | NOT PEER-REVIEWED | Posted: 23 August 2023 doi:10.20944/preprints202308.1671.v1

complex materials. The electrical properties conducted in wet condition which is more physiologically relevant showed low impedance at high frequencies due to capacitive currents (**Figure 17**). At lower frequencies, impedance decreased with increased CB content. Overall, impedance of the nanocomposite hydrogels decreased with increased CB concentrations. Additionally, the variance in electrical conductivity with and without biological cells along with various protocols is under progress. Since these nanocomposite hydrogels are prepared with the aim to develop novel scaffolds for tissue engineering applications, it is utmost important to evaluate the biocompatibility of these types of hydrogels, which is our future work. However, our previous studies on G/PEG/CH hydrogel using human mesenchymal stem cells (hMSCs) for assessing their tissue regeneration capability (chondrogenic and osteogenic differentiation) confirmed that this hydrogel scaffold was biocompatible and suitable for cell growth, chondrogenic and osteogenic differentiation, and mineralization [32,34].

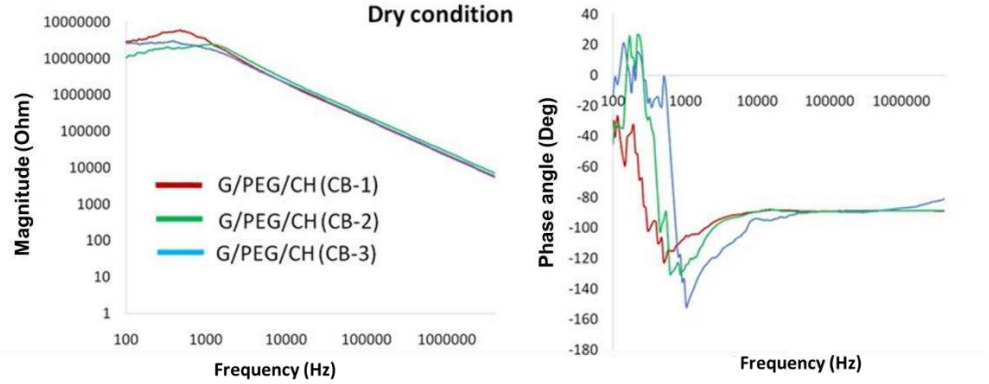

Figure 16. Complex impedance module and phase angles with respect to frequency of nanocomposite hydrogels tested in dry condition.

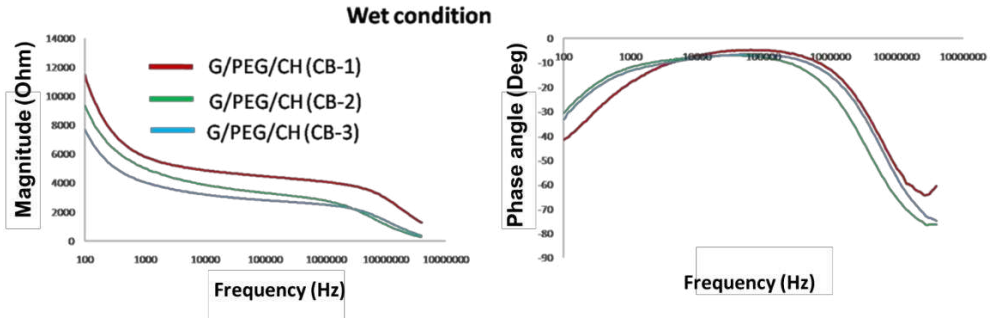

Figure 17. Complex impedance module and phase angles with respect to frequency of nanocomposite hydrogels tested in wet conditions.

4. Conclusions

Conductive nanocomposites have shown immense potential in tissue engineering due to their ability to support cell growth, promote tissue regeneration, and provide electrical stimulation to engineered tissues. These results revealed that the developed synthesis method was amenable enough to accommodate nanomaterials into macroporous hydrogels under mild conditions. Incorporation of conductive carbon black (CB) (10, 15 and 20 wt %) significantly improved electrical conductivity and enhanced mechanical properties with the increased CB content. Interestingly, nanocomposite hydrogel with 10 % CB provided both anisotropic morphology and mechanical property, whereas anisotropic pore morphology diminished at higher CB concentration (15 and 20 %) imparting denser texture. In general, under repeated compressive cyclic at 50 % deformation, all nanocomposite hydrogels showed nonlinear elasticity, toughness, preconditioning and characteristic hysteresis. Overall, the collective mechanical behavior resembled the mechanics of soft tissues. The electrical properties conducted in wet conditions, which is more physiologically relevant, showed

low impedance at high frequencies due to capacitive currents. Overall, impedance of the nanocomposite hydrogels decreased with increased CB concentrations. This work is still in the developing and optimizing stage. Finally, the combination of tissue-like morphological and mechanical behavior along with good electrical conductivity could lead to their use in various applications.

Author Contributions: Conceptualization, K.D. and L.S.; methodology, K.D.; E.S. and L.S.; formal analysis, K.D.; E.S.; A.G.; G.R. and L.S.; investigation, K.D.; E.S. and L.S.; data curation, K.D.; writing, E.S. and K.D.; writing—review and editing, K.D.; E.S.; A.G.; G.R. and L.S.; visualization, K.D.; A.G.; G.R. and L.S.; supervision, K.D. and L.S. All authors have read and agreed to the published version of the manuscript.

Funding: This research received no external funding.

Data Availability Statement: The raw/processed data required to reproduce these findings cannot be shared at this time as the data also forms part of an ongoing study.

Acknowledgments: N/A.

Conflicts of Interest: The authors declare no conflict of interest.

References

1. Dey, K., Roca, E., Ramorino, G., Sartore, L. Progress in the mechanical modulation of cell functions in tissue engineering. *Biomater. Sci.* **2020**, *8(24)*, 7033-7081.
2. Webber, M. J., Khan, O. F., Sydlik, S. A., Tang, B. C., Langer, R. A perspective on the clinical translation of scaffolds for tissue engineering. *Ann. Biomed. Eng.* **2015**, *43*, 641-656.
3. Lutolf, M. P., Gilbert, P. M., Blau, H. M. Designing materials to direct stem-cell fate. *Nature*, **2009**, *462*(7272), 433-441.
4. Okamoto, M., John, B. Synthetic biopolymer nanocomposites for tissue engineering scaffolds. *Prog. Polym. Sci.* **2013**, *38*(10-11), 1487-1503.
5. Alamdari, S. G., Alibakhshi, A., de la Guardia, M., Baradaran, B., Mohammadzadeh, R., Amini, M., Kesharwani, P., Mokhtarzadeh, A., Oroojalian, F., Sahebkar, A. (2022). Conductive and semiconductive nanocomposite-based hydrogels for cardiac tissue engineering. *Adv. Healthc. Mater.* **2022**, *11*(18), 2200526.
6. Guo, B., Ma, P. X. Conducting polymers for tissue engineering. *Biomacromolecules*. **2018**, *19*(6), 1764-1782.
7. Afjeh-Dana, E., Naserzadeh, P., Nazari, H., Mottaghitalab, F., Shabani, R., Aminii, N., Mehravi, B., Rostami, F.T., Joghataei, M.T., Mousavizadeh, K. Ashtari, K., 2019. Gold nanorods reinforced silk fibroin nanocomposite for peripheral nerve tissue engineering applications. *Int. J. Biol. Macromol.* **2019**, *129*, 1034-1039.
8. Ashtari, K., Nazari, H., Ko, H., Tebon, P., Akhshik, M., Akbari, M., Alhosseini, S.N., Mozafari, M., Mehravi, B., Soleimani, M. Ardehali, R. Electrically conductive nanomaterials for cardiac tissue engineering. *Adv. Drug Deliv. Rev.* **2019**, *144*, 162-179.
9. Esmaeili, H., Patino-Guerrero, A., Hasany, M., Ansari, M.O., Memic, A., Dolatshahi-Pirouz, A. Nikkhah, M. Electroconductive biomaterials for cardiac tissue engineering. *Acta Biomater.* **2022**, *139*, 118-140.
10. Chopra, V., Thomas, J., Kaushik, S., Rajput, S., Guha, R., Mondal, B., Naskar, S., Mandal, D., Chauhan, G., Chattopadhyay, N. Ghosh, D. 2023. Injectable bone cement reinforced with gold nanodots decorated rGO-hydroxyapatite nanocomposites, augment bone regeneration. *Small*, **2023**, *19*(14), 2204637.
11. Arambula-Maldonado, R. Mequanint, K. 2022. Carbon-based electrically conductive materials for bone repair and regeneration. *Mater. Adv.* **2022**, *3*(13), 5186-5206.
12. Asl, M.A., Karbasi, S., Beigi-Boroujeni, S., Benisi, S.Z. and Saeed, M. Polyhydroxybutyrate-starch/carbon nanotube electrospun nanocomposite: A highly potential scaffold for bone tissue engineering applications. *Int. J. Biol. Macromol.* **2022**, *223*, 524-542.
13. Mirmusavi, M.H., Ahmadian, M. Karbasi, S. 2022. Polycaprolactone-chitosan/multi-walled carbon nanotube: A highly strengthened electrospun nanocomposite scaffold for cartilage tissue engineering. *Int. J. Biol. Macromol.* **2022**, *209*, 1801-1814.
14. Huang, J., Liu, F., Su, H., Xiong, J., Yang, L., Xia, J. Liang, Y. Advanced nanocomposite hydrogels for cartilage tissue engineering. *Gels*, **2022**, *8*(2), 138.
15. Kwon, H.J., Lee, G.S. Chun, H. Electrical stimulation drives chondrogenesis of mesenchymal stem cells in the absence of exogenous growth factors. *Sci. Rep.* **2016**, *6*(1), 39302.
16. Shokrani, H., Shokrani, A., Jouyandeh, M., Seidi, F., Gholami, F., Kar, S., Munir, M.T., Kowalkowska-Zedler, D., Zarrintaj, P., Rabiee, N. Saeb, M.R. Green polymer nanocomposites for skin tissue engineering. *ACS App. Bio Mater.* **2022**, *5*(5), 2107-2121.
17. Elshishiny, F. Mamdouh, W. Fabrication of nanofibrous/xerogel layer-by-layer biocomposite scaffolds for skin tissue regeneration: in vitro study. *ACS Omega*, **2020**, *5*(5), 2133-2147.

18. Lim, C., Park, C., Sunwoo, S.H., Kim, Y.G., Lee, S., Han, S.I., Kim, D., Kim, J.H., Kim, D.H. Hyeon, T. Facile and scalable synthesis of whiskered gold nanosheets for stretchable, conductive, and biocompatible nanocomposites. *ACS Nano*, **2022**, *16*(7), 10431-10442.
19. Zare, E.N., Makvandi, P., Ashtari, B., Rossi, F., Motahari, A. Perale, G. Progress in conductive polyaniline-based nanocomposites for biomedical applications: a review. *J. Med. Chem.* **2019**, *63*(1), 1-22.
20. You, J.O., Rafat, M., Ye, G.J. Auguste, D.T. Nanoengineering the heart: conductive scaffolds enhance connexin 43 expression. *Nano Letters*, **2011**, *11*(9), 3643-3648.
21. Zhao, H., Liu, M., Zhang, Y., Yin, J. Pei, R. Nanocomposite hydrogels for tissue engineering applications. *Nanoscale*, **2020**, *12*(28), 14976-14995.
22. Mehrali, M., Thakur, A., Pennisi, C.P., Talebian, S., Arpanaei, A., Nikkhah, M. Dolatshahi-Pirouz, A. Nanoreinforced hydrogels for tissue engineering: biomaterials that are compatible with load-bearing and electroactive tissues. *Adv. Mater.* **2017**, *29*(8), 1603612.
23. Sakr, M.A., Sakthivel, K., Hossain, T., Shin, S.R., Siddiqua, S., Kim, J. Kim, K. 2022. Recent trends in gelatin methacryloyl nanocomposite hydrogels for tissue engineering. *J. Biomed. Mater. Res.* A. **2022**, *110*(3), 708-724.
24. Sun, H., Tang, J., Mou, Y., Zhou, J., Qu, L., Duval, K., Huang, Z., Lin, N., Dai, R., Liang, C. Chen, Z. Carbon nanotube-composite hydrogels promote intercalated disc assembly in engineered cardiac tissues through β1-integrin mediated FAK and RhoA pathway. *Acta Biomater.* **2017**, *48*, 88-99.
25. Shin, S.R., Zihlmann, C., Akbari, M., Assawes, P., Cheung, L., Zhang, K., Manoharan, V., Zhang, Y.S., Yüksekkaya, M., Wan, K.T. Nikkhah, M. Reduced graphene oxide-gelMA hybrid hydrogels as scaffolds for cardiac tissue engineering. *Small*, **2016**, *12*(27), 3677-3689.
26. Li, Y., Wei, L., Lan, L., Gao, Y., Zhang, Q., Dawit, H., Mao, J., Guo, L., Shen, L. Wang, L. Conductive biomaterials for cardiac repair: A review. *Acta Biomater.* **2022**, *139*, 157-178.
27. Moschou, E.A., Peteu, S.F., Bachas, L.G., Madou, M.J. Daunert, S. Artificial muscle material with fast electroactuation under neutral pH conditions. *Chem. Mater.* **2004**, *16*(12), 2499-2502.
28. Chuang, W.J., Chiu, W.Y. Tai, H.J. Temperature-dependent conductive composites: Poly (N-isopropylacrylamide-co-N-methylol acrylamide) and carbon black composite films. *J. Mater. Chem.* **2012**, *22*(38), 20311-20318.
29. Dey, K., Agnelli, S., Re, F., Russo, D., Lisignoli, G., Manferdini, C., Bernardi, S., Gabusi, E. Sartore, L. Rational design and development of anisotropic and mechanically strong gelatin-based stress relaxing hydrogels for osteogenic/chondrogenic differentiation. *Macromol. Biosci.* **2019**, *19*(8), 1900099.
30. Dey, K., Agnelli, S. Sartore, L. 2023, April. Designing viscoelastic gelatin-PEG macroporous hybrid hydrogel with anisotropic morphology and mechanical properties for tissue engineering application. *Micro*, **2023**, 3(2),434-457.
31. Dey, K., Agnelli, S., Borsani, E. Sartore, L. Degradation-dependent stress relaxing semi-interpenetrating networks of hydroxyethyl cellulose in gelatin-PEG hydrogel with good mechanical stability and reversibility. *Gels*, **2021**, *7*(4), 277.
32. Manferdini, C., Gabusi, E., Sartore, L., Dey, K., Agnelli, S., Almici, C., Bianchetti, A., Zini, N., Russo, D., Re, F. Mariani, E. Chitosan-based scaffold counteracts hypertrophic and fibrotic markers in chondrogenic differentiated mesenchymal stromal cells. *J. Tissue Eng. Regen. Med.* **2019**, *13*(10), 1896-1911.
33. Diani, J., Fayolle, B. Gilormini, P. A review on the Mullins effect. *Eur. Polym. J.* **2009**, *45*(3), 601-612.
34. Re, F., Sartore, L., Moulisova, V., Cantini, M., Almici, C., Bianchetti, A., Chinello, C., Dey, K., Agnelli, S., Manferdini, C. Bernardi, S. 3D gelatin-chitosan hybrid hydrogels combined with human platelet lysate highly support human mesenchymal stem cell proliferation and osteogenic differentiation. *J. Tissue Eng.* **2019**, *10*, 2041731419845852.